ChemComm

Accepted Manuscript

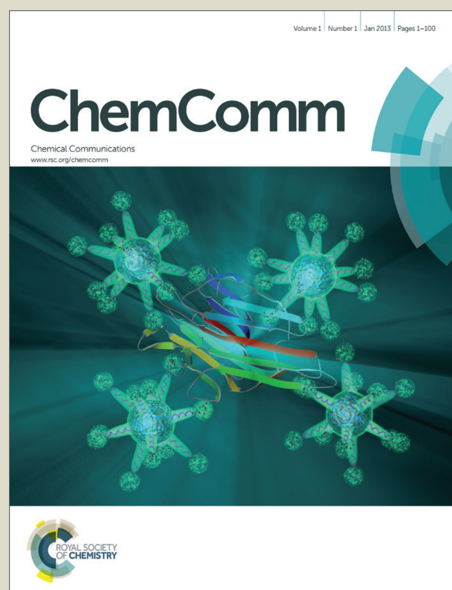

This is an *Accepted Manuscript*, which has been through the Royal Society of Chemistry peer review process and has been accepted for publication.

Accepted Manuscripts are published online shortly after acceptance, before technical editing, formatting and proof reading. Using this free service, authors can make their results available to the community, in citable form, before we publish the edited article. We will replace this *Accepted Manuscript* with the edited and formatted *Advance Article* as soon as it is available.

You can find more information about *Accepted Manuscripts* in the Information for Authors.

Please note that technical editing may introduce minor changes to the text and/or graphics, which may alter content. The journal's standard Terms & Conditions and the Ethical guidelines still apply. In no event shall the Royal Society of Chemistry be held responsible for any errors or omissions in this *Accepted Manuscript* or any consequences arising from the use of any information it contains.

ROYAL SOCIETY OF CHEMISTRY

www.rsc.org/chemcomm

Journal Name RSCPublishing

COMMUNICATION

Cite this: DOI: 10.1039/x0xx00000x

Received 00th January 2012,
Accepted 00th January 2012

DOI: 10.1039/x0xx00000x

www.rsc.org/

Non-uniform spatial distribution of tin oxide (SnO_2) nanoparticles at the air-water interface

Inga Jordan,[a] Amaia Beloqui Redondo,[b] Matthew A. Brown,[*b] Daniel Fodor,[b] Malwina Staniuk,[c] Armin Kleibert,[d] Hans Jakob Wörner,[a] Javier B. Giorgi,[e] and Jeroen A. van Bokhoven[b,d]

Depth resolved X-ray photoelectron spectroscopy (XPS) from a 25 µm liquid jet is used to quantify the spatial distribution of 3 nm SnO_2 nanoparticles (NPs) from the air-water interface (AWI) into the suspension bulk. Results are consistent with a layer several nm thick at the AWI that is completely devoid of NPs.

The attachment of NPs at liquid interfaces is a central topic in colloid science but remains poorly understood.[1] From a fundamental standpoint a well-defined NP at the air-liquid interface is viewed as an ideal system to investigate thermodynamic models, surface free energies, electrostatic interactions, capillary and solvation forces, line tensions, and phase behaviour.[1] Interest also arises from the commercial industry where NPs at liquid interfaces have applications stabilizing emulsions, foams, and microbubbles[2-4] that are commonplace in food, paint and cosmetics.[5] More recently, the nanotechnology sector has shown interest in NPs at liquid interfaces as a means to assemble complex 2d and 3d nanocrystal superlattices that possess unique chemical and physical properties for applications in electronic and optoelectronic devices such as LEDs, lasers, and solar cells.[6]

The attachment of NPs at air-liquid interfaces, that is their surface affinity, is traditionally characterized using surface tension measurements. These measurements rely on the Gibbs absorption equation[7] to calculate the interface density (Γ) from the recorded change in surface tension (dγ) with a change in chemical potential (dμ) of the adsorbing NPs, and have been performed successfully for over a half century.[8] While limitations such as lack of chemical and depth (subsurface) resolution preclude surface tension measurements from providing a complete microscopic description of NP attachment at and near the air-liquid interface, few analytic techniques offer improvement. With a clear desire to better understand NP attachment at liquid interfaces more refined microscopic probes are sought. Cryogenic electron tomography is to date the most successful and has recently been used to quantify the complete concentration gradient of oleic acid stabilized 5 nm PbSe NPs at the air-organic solvent interface.[9] Spectroscopic approaches remain to date largely unexplored.[10]

X-ray photoelectron spectroscopy (XPS) is a quantitative tool that offers depth resolution. By carrying out experiments as a function of incident photon energy, afforded by for example a synchrotron radiation facility, the probe depth of the experiment can be carefully controlled via the inelastic mean free path (IMFP)[11] of the outgoing photoelectron. Probe depths from a few molecular layers up to several tens of nm can be realized.[11] Only recently however has XPS been extended to aqueous samples using a liquid microjet[12] and its application to interrogate the three-way interface of air-water-NP is a relatively virgin discipline[13-16] with but a single depth-resolved study that did not attempt to quantify NP spatial distributions.[17] Here we combine XPS with a liquid microjet operating on a colloidal SnO_2 suspension to measure depth-resolved NP spatial distributions at the AWI. The present report is the first attempt to quantify NP spatial distributions at the AWI using a spectroscopic method.

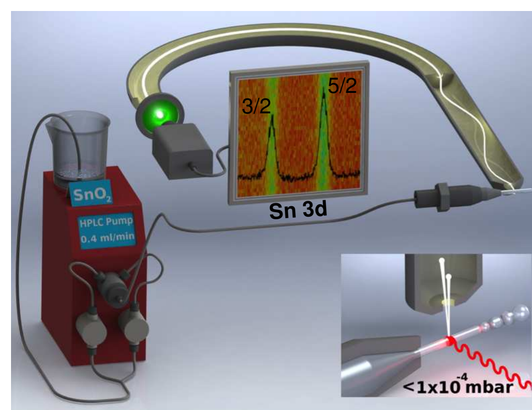

Fig. 1. Setup used to perform depth-resolved X-ray photoelectron spectroscopy measurements at the three-way interface of air-water-nanoparticle. Colloidal suspensions of 7.5 wt % SnO_2 are injected into the measurement chamber using a fused quartz capillary with diameter 25 µm. (Inset) Experimental geometry.

Our experimental model system consists of charge-stabilized colloidal SnO_2. These NPs are ligand-free and rely on the electric field generated at the particles' surface by (de)protonated hydroxyl groups for stability. SnO_2, a wide band gap semiconductor, has applications in gas sensing, catalysis, electrochemistry, and

ChemComm Accepted Manuscript

optoelectronic devices.[18] Colloidal suspensions of SnO_2 are used to generate nanocrystalline thin films that have been successful in dye sensitization for solar cell technology.[19] As such, a microscopic description of SnO_2 NPs in liquid solutions will benefit several scientific disciplines of current significance.

The setup of our liquid microjet experiment at the SIM beamline[20] of the Swiss Light Source is shown in Fig. 1. The experiment uses a NAPP spectrometer[21] operating at constant pass energy of 50 eV for all photoelectron kinetic energies (pKE). The direction of liquid microjet flow, incident photon, and photoelectron detection are orthogonal (inset of Fig. 1). Suspensions of 7 wt % SnO_2 are prepared by diluting a commercially available 15 wt % sample (Nyacol SN15). The suspension pH is 10.5 and particle diameters are 3.0 ± 1.6 nm as determined by in situ small angle X-ray scattering (ESI). Representative TEM micrographs of dried (ex situ) aliquots of the suspension are found in the ESI. Sn $3d_{5/2}$ spectra are collected from a 25 µm liquid jet operating at 279 K and a flow rate of 0.4 mL/min. The diameter of the liquid jet, the liquid flow rate, and the pressure inside the ionization chamber are not expected to influence the results of the present study.[13] Measurements are carried out at pKEs of 110, 210, 310, 435, 580, and 810 eV using incident photon energies of 600, 700, 800, 925, 1070, and 1300 eV, respectively. Collection time is typically 25 min/spectrum, although at 110 and 210 eV pKE the signal is averaged for 50 mins to increase the signal to noise. The probe depth of the experiment is a strong function of pKE[21] and is only beginning to be understood in aqueous solutions.[22] A well-pronounced minimum is believed to occur around 100 eV,[21] and with increasing pKE the probe depth increases. We use IMFP of 7.8 Å (110 eV pKE), 10.4 Å (210 eV), 13.3 Å (310 eV), 17.0 Å (435 eV), 19.5 Å (580 eV), and 27.2 Å (810 eV).[22]

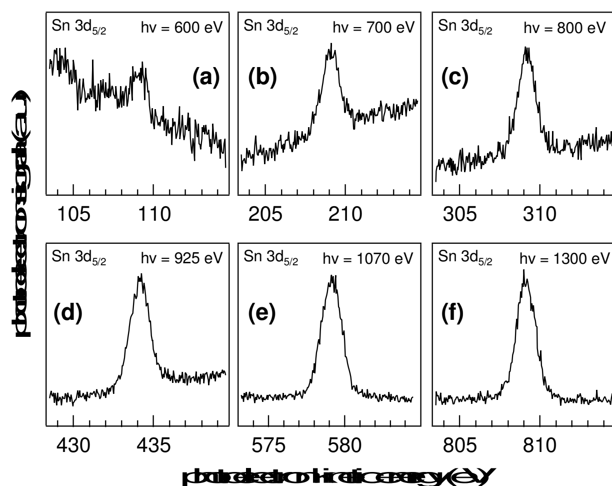

Fig. 2. Sn $3d_{5/2}$ XP spectra as a function of photoelectron kinetic energy (pKE). (a) 110 eV, (b) 210 eV, (c) 310 eV, (d), 435 eV, (e) 580 eV, and (f) 810 eV. Raw data are shown. To quantify the spectral intensity a Gaussian function is fit to each spectrum following a linear background subtraction and the integrated intensity normalized to photon flux, photoionization cross section, and analyser transmission function.

Fig 2 shows the as-collected Sn $3d_{5/2}$ spectra at pKE of (a) 110, (b) 210, (c) 310, (d) 435, (e) 580, and (f) 810 eV. Relatively poor signal quality (despite the highest photon flux and photoionization cross-section[23]) at 110 eV pKE is a direct reflection of the spatial distribution of the NPs at the AWI (vide infra). The complete Sn 3d orbital with both the $3d_{5/2}$ and $3d_{3/2}$ components is shown in Fig. 1. Here we use only the $3d_{5/2}$ component for determining SnO_2 NP spatial distributions at the AWI. The XP spectra can be quantified by normalizing the integrated intensity following background subtraction to photon flux, photoionization cross-section,[23] and to the transmission function of the hemispherical NAPP spectrometer. The normalized intensity is shown in Fig. 3a (black markers) as a function of IMFP. The value at 27.2 Å (810 eV pKE) has been set to unity for simplicity. The normalized intensity is relatively flat between 7-13 Å after which it increases sharply up to 27.2 Å. Error bars represent the standard deviation of repeat measurements.

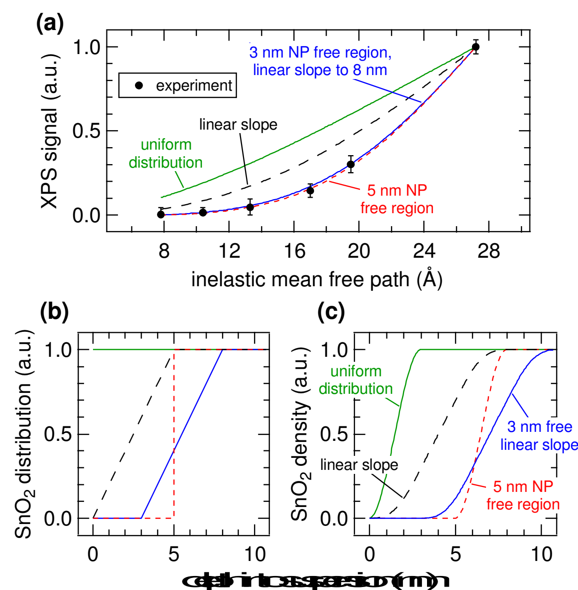

Fig. 3. (a) Measured (markers) and calculated (lines) signal intensities as a function of inelastic mean free path (IMFP). (b) Four different NP spatial distribution models and (c) their corresponding density profiles. The air-water interface is at a depth of 0 nm in (b) and (c).

The normalized XPS intensities as a function of IMFP can be compared with the predicted signals from different NP distributions at the AWI. A uniform distribution of randomly oriented SnO_2 NPs (Fig. 3b, green trace) from the AWI into the bulk gives rise to the density profile of Fig. 3c (green trace, uniform distribution). Bulk suspension SnO_2 density is realized at a depth below the AWI equal to the NP diameter (in this case 3 nm). The density profile of the uniform NP distribution can be integrated using well-established methods[14, 17, 24-26] to generate a predicted XPS intensity as a function of IMFP that can be directly compared with the experimental values.

The integral takes the form $\int_0^\infty e^{\frac{-z}{IMFP}}\rho(z)dz$ where IMFP is the inelastic mean free path, z is the distance into suspension from the AWI, and ρ(z) is the SnO_2 density at a given depth. The limits of the integral are from the AWI into the bulk. In theory this calculation is a double integral[17] where an IMFP for SnO_2 is first used to calculate the attenuation of the PE within the NP, and a second integral uses IMFP for liquid water to account for further attenuation in the condensed liquid phase before the PE escapes into vacuum. In practice, and as we show in the ESI, variations of ± 25% in the IMFP have very little effect on the results of this study and the equation can be simplified to the single integral shown. The predicted XPS intensity for a uniform NP distribution over IMFP spanning the experimental range is shown in Fig. 3a (green trace, uniform distribution). The experimental intensities are grossly overestimated for all IMFP. This result suggests that the NPs do not have a uniform distribution near the AWI but are instead depleted relative to the bulk. Density profiles (Fig. 3c) and predicted XPS intensities (Fig.

ChemComm Accepted Manuscript

This journal is © The Royal Society of Chemistry 2012

3a) have been similarly calculated for NP distributions (Fig. 3b) that include a 5 nm thick region at the AWI where the NPs are completely excluded followed by a step function increase in distribution to the bulk value (red dotted trace), for a linear increase in NP distribution from zero depth to 5 nm (black dashed trace), and for a distribution that includes an excluded region (3 nm) followed by a linear increase to a depth of 8 nm (blue trace). As seen in Fig. 3a the experimental intensities are well reproduced only by distribution models that include a region at the AWI where the NPs are completely excluded. Models that use a linear increase in NP distribution (e.g., black dashed trace) from zero depth, irrespective of slope (we have modelled slopes that extend to depths of 15 nm), cannot reproduce the experimental intensities. The XPS results are consistent with NP distributions at the AWI that include a region 3-5 nm thick where the SnO_2 NPs are completely excluded.

There remains uncertainty in the energy dependence of the IMFP in liquid water.[22, 27] To help account for this uncertainty and to justify our simplification of the predicted XPS intensities to a single integral, we have calculated SnO_2 NP spatial distributions using IMFP of ± 25% (ESI). The experimental results are consistent with NP free regions of 2-3.5 nm (−25%) and 4-6.5 nm (+25%). Uniform distributions and models that include a linear increase in distribution from zero depth again do not reproduce the experimental results. Irrespective of IMFP, all NP distribution models that reproduce the experimental intensities require a layer at the AWI that is completely devoid on NPs.

Exclusion of charge-stabilized oxide NPs from the AWI is not unprecedented and has been shown both theoretically[28] and experimentally[14] to originate from electrostatic interaction between the charged NP and the charged AWI. Under the conditions of our experiment both the SnO_2 NPs and the AWI have negative charge and electrostatic repulsion is expected. What does, however, appear surprising are the large depths by which the NPs are excluded. Accounting for uncertainty in the IMFP of liquid water, our results indicate that 3 nm SnO_2 NPs reside below at least 6 molecular layers of water at the AWI.

In summary, we have demonstrated that energy-dependent XPS from a liquid microjet can be used to quantify the depth-resolved spatial distributions of NPs at the AWI. Charge-stabilized SnO_2 NPs are completely excluded from the AWI, with similar behaviour expected for many other types of surfactant-free NPs in aqueous suspensions. In addition to the fundamental benefits of these types of measurements, the chemical sensitivity of XPS will allow for the spatial distributions of different composition NPs in a nanocrystal superlattice to be individually determined during the assembly phase.

A portion of this work was performed at the Swiss Light Source, Paul Scherrer Institute, Villigen, Switzerland. I.J. acknowledges support from ETH-FAST as part of the NCCR MUST program.

Notes and references

[a] Laboratory of Physical Chemistry and [b] Institute for Chemical and Bioengineering and [d] Department of Materials, ETH Zürich. [d] Paul Scherrer Institute. [e] CCRI and Department of Chemistry, University of Ottawa. E-mail: matthew.brown@chem.ethz.ch

Electronic Supplementary Information (ESI) available: SAXS curve and fit, TEM micrographs, XPS fits, and an analysis of NP spatial distributions using ± 25% IMFP. See DOI: 10.1039/c000000x/

1. F. Bresme and M. Oettel, *J Phys-Condens Mat*, 2007, 19, 413101.
2. R. Aveyard, B. P. Binks and J. H. Clint, *Adv Colloid Interfac*, 2003, 100, 503-546.
3. B. P. Binks, *Curr Opin Colloid In*, 2002, 7, 21-41.
4. B. P. Binks and T. S. Horozov, *Angew Chem Int Edit*, 2005, 44, 3722-3725.
5. E. Dickinson, *Curr Opin Colloid In*, 2010, 15, 40-49.
6. D. Vanmaekelbergh, *Nano Today*, 2011, 6, 419-437.
7. H.-J. Butt, K. Graf and M. Kappl, *Physics and Chemistry of Interfaces*, Wiley-VCH Verlag GmbH & Co, Weinheim, 3rd edn., 2013.
8. H. Salmang, W. Deen and A. Vroemen, *Berichte der Deutschen Keramischen Gesellschaft*, 1957, 34, 34-38.
9. J. van Rijssel, M. van der Linden, J. D. Meeldijk, R. J. A. van Dijk-Moes, A. P. Philipse and B. H. Erne, *Phys Rev Lett*, 2013, 111, 108302.
10. M. Paulus, P. Degen, S. Schmacke, M. Maas, R. Kahner, B. Struth, M. Tolan and H. Rehage, *Eur Phys J-Spec Top*, 2009, 167, 133-136.
11. C. J. Powell and A. Jablonski, *NIST Electron Inelastic-Mean-Free-Path Database,* National Institute of Standards and Technology, Gaithersburg, MD, Version 1.1 edn., 2000.
12. B. Winter and M. Faubel, *Chem Rev*, 2006, 106, 1176-1211.
13. M. A. Brown, A. Beloqui Redondo, M. Sterrer, B. Winter, G. Pacchioni, Z. Abbas and J. A. van Bokhoven, *Nano Letters*, 2013, 13, 5403-5407.
14. M. A. Brown, N. Duyckaerts, A. Beloqui Redondo, I. Jordan, F. Nolting, A. Kleibert, M. Ammann, H. J. Woerner, J. A. van Bokhoven and Z. Abbas, *Langmuir*, 2013, 29, 5023-5029.
15. M. A. Brown, I. Jordan, A. Beloqui Redondo, A. Kleibert, H. J. Wörner and J. A. van Bokhoven, *Surf Sci*, 2013, 610, 1-6.
16. J. Soderstrom, N. Ottosson, W. Pokapanich, G. Ohrwall and O. Bjorneholm, *J Elec Spec Rel Phenom*, 2011, 184, 375-378.
17. M. A. Brown, R. Seidel, S. Thurmer, M. Faubel, J. C. Hemminger, J. A. van Bokhoven, B. Winter and M. Sterrer, *Phys Chem Chem Phys*, 2011, 13, 12720-12723.
18. J. Ba, J. Polleux, M. Antonietti and M. Niederberger, *Adv Mater*, 2005, 17, 2509-2512.
19. S. Ferrere, A. Zaban and B. A. Gregg, *J Phys Chem B*, 1997, 101, 4490-4493.
20. U. Flechsig, F. Nolting, A. F. Rodriguez, J. Krempasky, C. Quitmann, T. Schmidt, S. Spielmann and D. Zimoch, *AIP Conference Proceedings*, 2010, 1234, 319-322.
21. M. A. Brown, et al., *Rev Sci Instruments*, 2013, 84, 073904.
22. S. Thurmer, R. Seidel, M. Faubel, W. Eberhardt, J. C. Hemminger, S. E. Bradforth and B. Winter, *Phys Rev Lett*, 2013, 111, 173005.
23. J. J. Yeh and I. Lindau, *Atom Data Nucl Data*, 1985, 32, 1-155.
24. M. A. Brown, R. D'Auria, I. F. W. Kuo, M. J. Krisch, D. E. Starr, H. Bluhm, D. J. Tobias and J. C. Hemminger, *Phys Chem Chem Phys*, 2008, 10, 4778-4784.
25. M. A. Brown, B. Winter, M. Faubel and J. C. Hemminger, *J Am Chem Soc*, 2009, 131, 8354-8355.
26. M. H. Cheng, K. M. Callahan, A. M. Margarella, D. J. Tobias, J. C. Hemminger, H. Bluhm and M. J. Krisch, *J Phys Chem C*, 2012, 116, 4545-4555.
27. N. Ottosson, M. Faubel, S. E. Bradforth, P. Jungwirth and B. Winter, *J Elec Spec Rel Phenom*, 2010, 177, 60-70.
28. A. Shrestha, K. Bohinc and S. May, *Langmuir*, 2012, 28, 14301-14307.

ChemComm Accepted Manuscript

Table of Contents Entry:

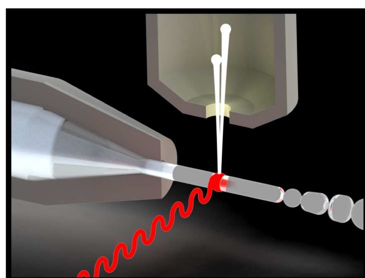

Nanoparticle spatial distributions are determined at the air-water interface using X-ray photoelectron spectroscopy from a liquid microjet.

ChemComm Accepted Manuscript

This journal is © The Royal Society of Chemistry 2012